Trans Indian Inst Met (2014) 67(4):521–530
DOI 10.1007/s12666-013-0375-2

TECHNICAL PAPER

TP 2781

Hot Deformation Behaviour of AA2014–10 wt% SiC Composite

Aruna Patel · S. Das · B. K. Prasad

Received: 30 May 2013 / Accepted: 20 December 2013 / Published online: 12 January 2014

Abstract The hot compression behaviour of AA2014 alloy having 10 wt% SiC particles was studied over a wide range of temperatures (ambient to 400 °C) and strain rates (0.01–10/s). The results were compared with those obtained from identical tests performed on the base alloy to understand the effect of the SiC particle reinforcement. Processing maps were generated using dynamic materials model from the flow stress of the samples. Microstructures of the deformed samples suggest the occurrence of dynamic recrystallization at high temperatures and low strain rate. Flow localization and adiabatic shear bands were observed at higher strain rates and temperatures. The lack of cohesion between SiC particles and the matrix was found to be responsible for the deteriorating deformation behavior of the composite over most of the processing domains. The activation energy for high temperature deformation in the presence of the SiC particles in the alloy was found to be significantly higher than that of the matrix. This makes deformation processing of the composite more difficult than that of the matrix.

Keywords Al composite · Compressive deformation · Processing map · Microstructure strain rate · Zener–Hollomon parameter · Activation energy

1 Introduction

Cast Al alloy composites reinforced with hard ceramic particles are recognized as a potential material system for automobile and aerospace applications because of their interesting combinations of properties such as higher specific strength, higher specific modulus, and excellent wear resistance in addition to light weight [1–3]. In the recent past, considerable attempts have been made to translate lightweight cast Al composites into meaningful components such as brakedrum, brake disc, connecting rod, piston, armor, etc. [4–7]. However, dispersion of fine reinforcement particles makes the composites a potential material system for structural applications [8, 9]. The requirement of high strength and other superior mechanical properties necessitates secondary deformation of the composites. Some of the deformation processes include extrusion, rolling, forging, equichannel angular pressing, etc. [10–16]. Needless to say, dispersed ceramic particles largely restrict the plastic flow of the alloy. To carry out secondary deformation of Al composites, one has to carefully select the deformation parameters like temperature and strain rate to achieve defect free components. This requires carrying out a substantial number of experiments. Generation of processing maps based on dynamic materials model (DMM) originally proposed by Prasad and Sasidhara [17], Raj [18], Gandhi [19], and Gandhi and Raj [20] helps to predict the safe and unsafe processing domains. In some of the recent studies, it is mentioned that the microstructural investigation of hot deformed Al composites showed dynamic recovery (DRV) as the predominant restoration mechanism [21–24]. In the case of 6XXX and 2XXX series alloys and composites, dynamic recrystallization (DRX) has been found to occur at temperatures closed to 500 °C as the predominating mechanism of deformation [21–23]. Vedani et al. [24] have studied the mechanical and tensile fracture behaviour of AA6061 and AA2618 reinforced with Al_2O_3 and SiC particles and inferred that microvoid formation due to particle fracture is the mechanism of failure of material at room temperature and 350 °C whereas particle/matrix debonding becomes the

A. Patel · S. Das (✉) · B. K. Prasad
CSIR-Advanced Materials and Processes Research Institute, Bhopal 462026, India
e-mail: sdas88@hotmail.com; sdas@ampri.res.in

predominant mechanism of material failure at higher temperatures. Cerri et al. [25] have shown that breaking of particles due to stress accumulation is the main reason for instability in the case of cast, homogenized and extruded 6061–Al_2O_3 composite. Bhat et al. [26] have indicated the occurrence of superplasticity in the strain rate range of 0.01–0.001/s and temperature 450–500 °C in the case of 2014–20 vol% Al_2O_3 composite. Localized shear bands and cracking were the mechanisms of failure of composite at strain rates greater than 1/s and temperature below 350 °C. Murty et al. [27] have suggested the optimum condition for the hot working of the as cast and extruded AA2014–20 vol% Al_2O_3 composite to be 500 °C and 0.001/s. Shao et al. [28] have shown that the general configuration of processing maps generated for the powder processed AA2024–20 vol% SiC composite based on DMM and modified DMM has been found to be similar. Their study revealed large un-stable regions in the form of flow localization and cavitation located at the matrix/SiC particle interface and within the SiC particle clusters. Ganesan et al. [29] have observed shear band formation and particle fracture to be the main reason for failure in the case of 6061 Al–15 % SiC composite at low temperature and higher strain rate. Bhat et al. [30] observed the occurrence of superplasticity and DRX at 525 °C at the strain rates of 0.001 and 10/s, respectively in the case of compression testing of P/M processed and subsequently extruded 2014–20 vol% SiC composite. The composite containing 15 vol% SiC was noted to be the ideal for showing superplasticity. In an another study, P/M hot pressed 2124–15 % SiC composite showed poor efficiency of power dissipation [31]. DRX was found to occur in the temperature range of 360–460 °C and strain rates of 0.1–0.7/s. At higher strain rates, particle cracking and shear band formation were observed [31]. Xiao et al. [32] showed that flow instability occurs due to adiabatic shear band formation in the temperature range of 350–500 °C and strain rate of 0.3–10/s in the case of P/M processed AA2009–15 vol% SiC composite. However, deformation at higher temperatures (500 °C) and lower strain rates (0.001/s) showed the highest efficiency of power dissipation leading to the generation of recrystallized grains.

An appraisal of the observations made in earlier studies shows no direct correlation between the operating mechanisms and the test and material related conditions. This could be attributed to the sensitivity of the deformation behaviour of materials towards a number of parameters like prior processing history, composition, microstructure, etc. of the starting material. Accordingly, it becomes imperative to assess the deformability characteristics of materials on a case-to-case basis.

In view of the above, an attempt has been made in the present work to study the hot working behavior of 2014 alloy and its composite containing 10 wt% SiC particles. Microstructure of the deformed samples was studied to understand the material failure mechanism at different temperatures and strain rates. A detailed investigation has also been carried out to examine the process of fracture in the samples as a function of temperature and strain rate. The inferences of the processing maps in different domains of processing have been validated through the microstructural features of the samples. Further, the deformation parameters have been correlated with Zener–Hollomon parameter and activation energy needed for hot deformation estimated.

2 Experimental

In the present study, 2014 Al alloy (Al–4.4Cu–0.97 Mg) was used as the matrix material. 10 wt% SiC particles (size 10–40 μm) were dispersed in the alloy melt by stir casting technique for synthesizing the composite. The melt was solidified in a cast iron mould to shape it in the form of 20 mm diameter and 200 mm long cylindrical samples. The samples were homogenized at 400 °C for 12 h. The homogenized samples were machined in the form of 10 mm diameter and 15 mm long specimens for compression testing. The compression tests were conducted employing a universal testing machine (Model: BISS 50 KN, Make: BISS Bangalore, India) at different temperatures (ambient to 400 °C) and strain rates (0.01–10/s). The samples were preheated in between the compression platens for 10 min prior to loading with a view to realize a uniform level of heating throughout the sample being tested. Microstructural features of the samples were studied using scanning electron microscope (Model: JSM-5600, Make: JEOL Japan). For microstructural observations, the deformed samples were cut, polished using standard metallographic practices, etched with Keller's reagent and coated with gold.

Processing maps were generated by the superimposition of the variation of the efficiency of power dissipation (η) towards microstructure evolution during deformation and instability parameter $\Sigma(\dot{\xi})$ with temperature and strain rate. The approach follows the dynamic material model (DMM) that considers the machine as the source of power and the material as the power dissipater. The efficiency of power dissipation and instability parameter were computed at specific strains using the flow stress data at different strain rates and temperatures using the following equations:

$$\eta = 2m/m + 1 \tag{1}$$

$$\Sigma\left(\dot{\xi}\right) = \{\partial \ln(m/(m+1))/\partial \ln \dot{\epsilon}\} + m \leq 0 \tag{2}$$

where σ, $\dot{\varepsilon}$, and m stand for flow stress, true strain rate and strain-rate sensitivity parameter, respectively.

3 Results

3.1 Flow Behaviour

The true stress–true strain diagram of AA2014 and AA2014–10 wt% SiC composites at various temperatures and strain rates are shown in Figs. 1 and 2, respectively. It is seen that the true stress increases with true strain to a peak value and then it becomes constant (Figs. 1a, c, 2a, b), decreases (Figs. 1b, d, 2c, d) or increases at a slow rate (Figs. 1a, 2a) with a further increase in strain. It is observed that flow stress increases with increasing strain rate and decreases with increasing temperature. Figure 1a shows the effect of temperature on AA2014 at a strain rate 0.01/s. It is noted that peak stress is around 375 MPa at a temperature of 30 °C and on increasing the test temperature to 200 °C, the peak stress is decreased to 290 MPa. On further increasing the test temperature to 400 °C, the peak stress is decreased to 68 MPa. Similarly, Fig. 1b shows the effect of temperature of AA2014–10 wt% SiC composite at strain rate of 0.01/s. The peak stress at 30 °C is noted to be around 360 MPa, and on increasing the temperature the peak stress is reduced to 250 MPa. Further increasing the temperature to 400°C it reduced to 50 MPa. The results clearly indicated that by dispersing SiC particles in AA2014, the peak stress is decreased. Similarly Fig. 1c, d shows the stress–strain curve of AA2014 and AA2014–10 wt% SiC composite, tested at strain rate of 10/s. It is observed that in AA2014 the peak stress at 30 °C is around 360 MPa which is reduced to 120 MPa at 400 °C. In AA2014–10 wt% SiC composite, the peak stress is found 345 MPa which reduced to 115 MPa at 400 °C. These observations clearly indicated that after adding SiC particle in AA2014 the peak stress is reduced at all temperatures.

Figure 2a, b shows the effect of strain rate on the compressive stress of AA2014 and AA2014–10 wt% SiC composite tested at room temperature respectively. It is noted that peak stress increases with increasing strain rate. For example AA2014 alloy tested at room temperature (30 °C) reaches to a peak stress of 350 MPa at strain rate of 0.01/s, which increased to 380 MPa when the sample is tested at 10/s. Similarly the peak stress of AA2014–10 wt% composite, at room temperature is found to be 330 MPa at 0.01/s, which increased to 375 MPa at 10/s. Further at higher temperature say 400 °C, the peak stress is found 68 MPa and is increased to 120 MPa at strain rate of 0.01 and 10/s for AA2014 alloy respectively. Similarly in AA2014–10 wt% SiC composite, the peak stress is 50 MPa at 0.01/s which increased to 115 MPa at 10/s at a temperature of 400°C. These trends of variations are shown in Fig. 2c, d. Figure 1a, b shows the peak stress values of

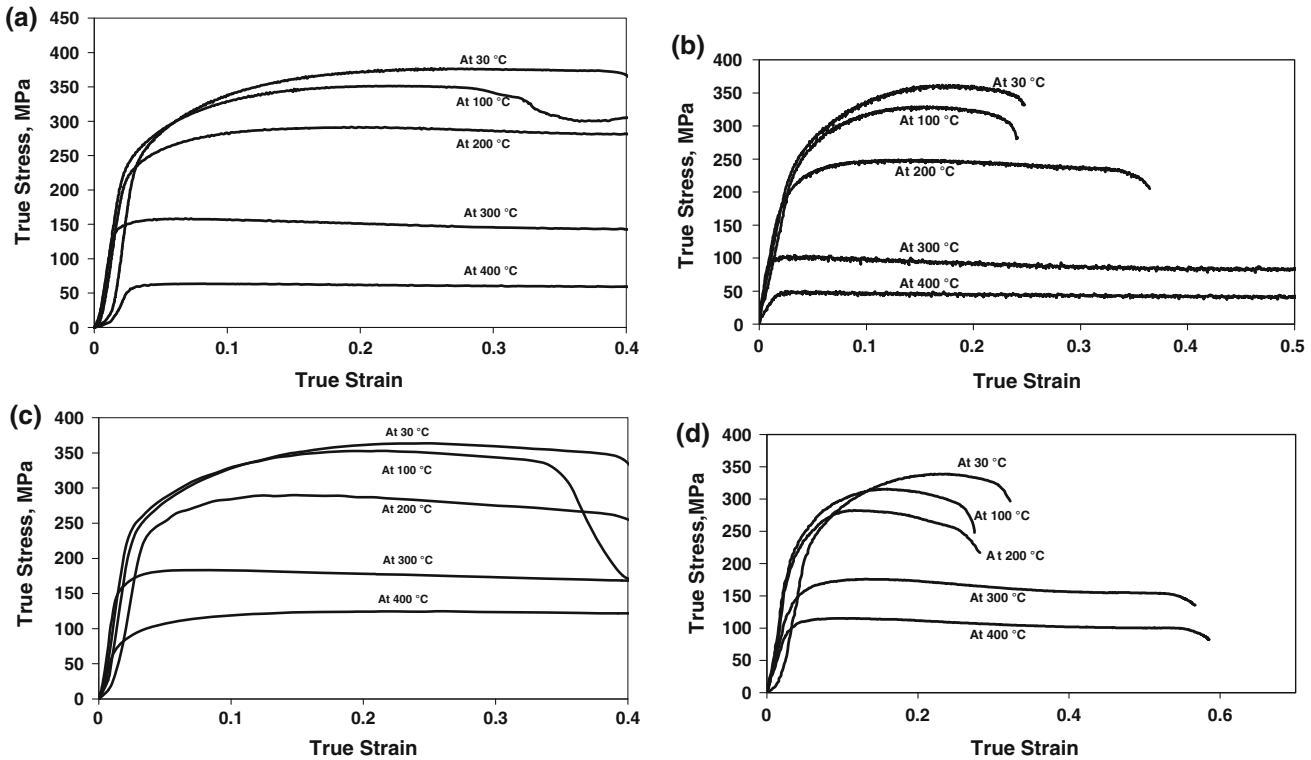

Fig. 1 Effect of temperature on flow behavior of AA2014 alloy and AA2014–10 wt% SiC composite **a** AA2014 alloy at 0.01/s, **b** AA2014–10 wt% SiC composite at 0.01/s. **c** AA2014 alloy at 10/s, **d** AA2014–10 wt% SiC composite at 10/s

AA2014 and AA2014–10 % SiC composite at various strain rate and temperature.

3.2 Processing Maps

Figure 3 shows the processing maps of the samples at a typical strain of 0.2. The positive integers and negative fractions in the figure represent the values of η (in %) and $\Sigma(\dot{\xi})$ respectively. Processing maps provide limiting temperature and strain rate condition for the initiation of fracture and instability. The optimum hot working condition for safe deformation of the matrix alloy is found at 350–400 °C and strain rates 0.01–0.1/s with η falling in the range of 40–80 %, η increasing with the lowering of strain rates and a rise in temperature (Fig. 3a). At low temperature 100–200 °C and 0.01–0.1/s strain rate alloy also shows safe deformation domain with η in the range of 35–50 %. Flow instability in this case was noted in the temperature range of (a) ambient-400 °C and strain rates of 0.1–10/s and (b) ambient-80 and 225–350 °C and strain rate 0.01–0.1/s. It may be noted that adding SiC particles to the matrix alloy decreased η from 40–80 to 5–35 % for safe deformation (Fig. 3a vs b). In case of the composite, safe processing domain was noted in the temperature range of 300–400 and 75–200 °C and strain rate 0.01–0.1 and 0.15–5/s respectively, while flow instability occurred in the temperature range of (a) 30–280 °C and strain rate range 0.01–0.15/s and (b) 250–400 °C and 0.1–10/s strain rate (Fig. 3b).

3.3 Microstructural Features

Figure 4a shows the typical microstructure of AA2014 alloy deformed at 30 °C at a strain rate of 0.01/s. The matrix microstructure of AA2014 shows Al dendrites and Al–$CuAl_2$ phase in the interdendritic region. Figure 4b shows the microstructure of AA2014 alloy deformed at 30 °C at a strain rate of 10/s. It shows the elongated grains with flow localization (Shown by arrow marks). Testing the samples at 400 °C and 0.01/s strain rate, showed the formation of fine precipitates in the matrix (Fig. 4c) and recrystallized grains were noticed, whereas at higher strain rate adiabatic shear bands were observed (Fig. 4d). The microstructural study clearly reveals that deformation at low temperature and low strain rate is realized through flow localization while at low temperature and high strain rate, adiabatic shear band formation is observed. DRX is the flow mechanism observed at high temperature and low

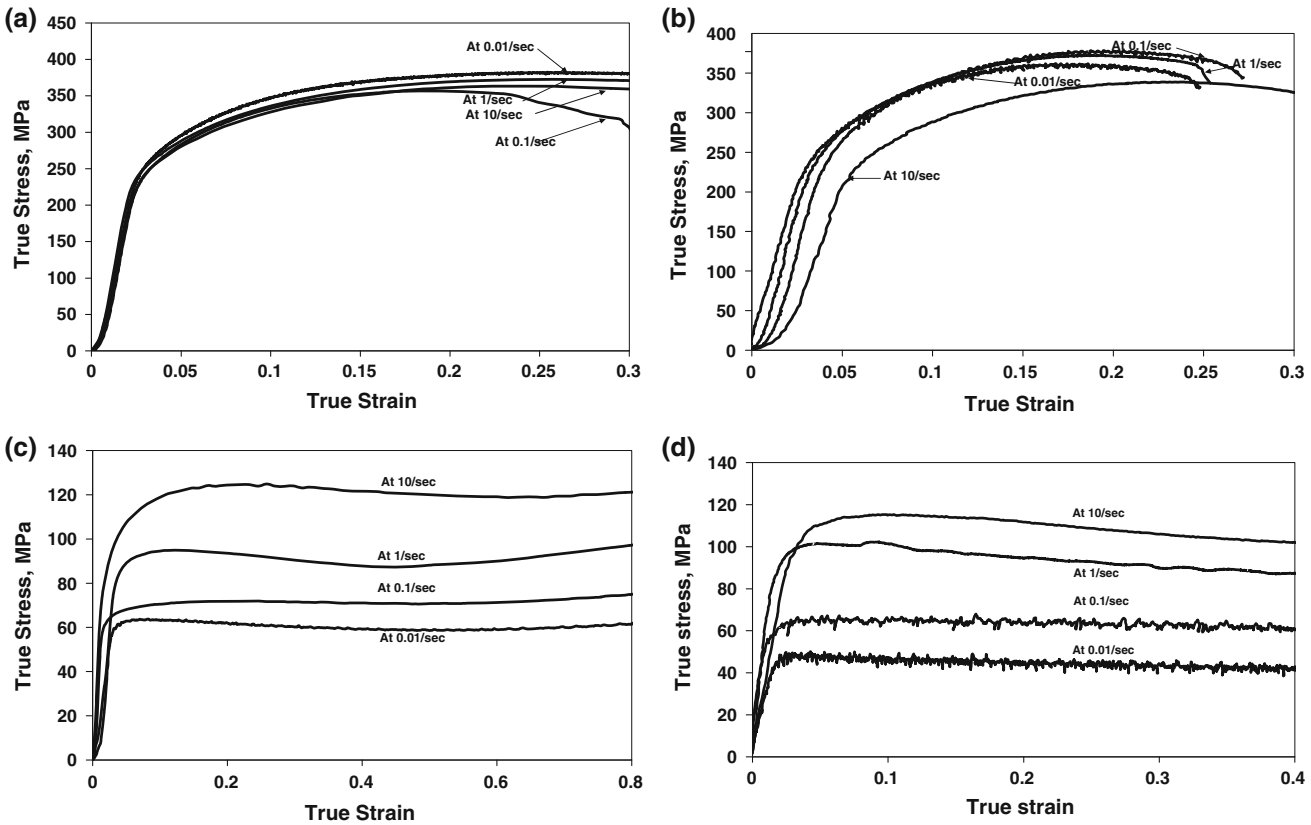

Fig. 2 Effect of strain rates on flow behavior of AA2014 alloy and AA2014–10 wt% SiC composite **a** AA2014 alloy at 30 °C, **b** AA2014–10 wt% SiC composite at 30 °C. **c** AA2014 alloy at 400 °C, **d** AA2014–10 wt% SiC composite at 400 °C

strain rate of deformation. Studying the samples in the temperature range of 100–200 °C and 0.01–0.1/s strain rate showed decohesion as the major failure mechanism. The higher efficiency (35–50 %) showed over here is due to decohesion at the matrix alloy/SiC interface.

Figure 5 shows the micrographs of the composite deformed at different temperatures and strain rates. Flow localization revealing banded structure along with alignment of SiC particles in the direction of flow at the ambient temperature and 0.01/s strain rate (Fig. 5a). Decohesion at the matrix/dispersoid interface and fragmentation of the dispersoid phase were also seen (Fig. 5b). A higher magnification micrograph clearly shows the interfacial debonding (Fig. 5c). Elongated grains with adiabatic shear band formation were observed at a higher strain rate of 10/s at the (ambient) temperature (Fig. 5d). The samples deformed at 400 °C and strain rate of 10/s showed elongated grains and SiC particle/matrix interfacial decohesion (Fig. 5e). On the contrary, fine equiaxed DRX grains in the matrix along with interfacial decohesion were noticed at a temperature of 400 °C at a strain rate of 0.01/s (Fig. 5f). Thus, deformation at low temperatures and strain rates leads to flow localization and interfacial decohesion. On contrary, low temperature and high strain rate deformation gives rise to shear band formation and strong interfacial decohesion. DRX is the flow mechanism observed at high temperatures and low strain rates which is supported by the formation of submicron size DRX grains.

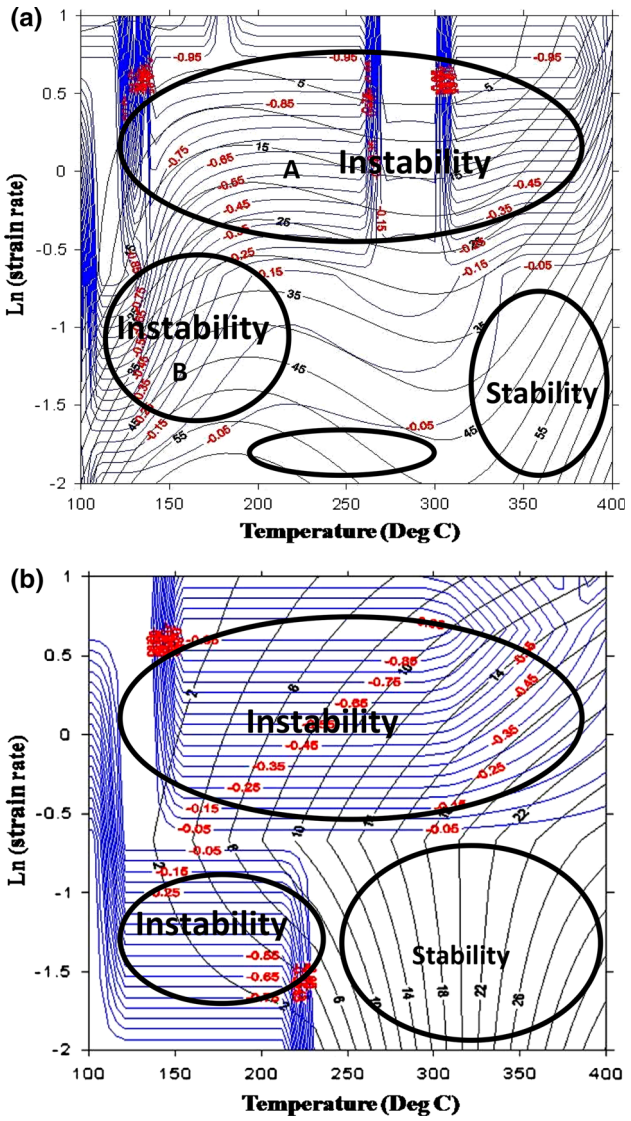

Fig. 3 Processing map of **a** AA2014 alloy and **b** AA2014–10 % SiC composite at 0.2 strain showing the different domain

4 Discussion

From microstructural standpoint, the dispersed SiC particles impart higher thermal stability and hardness to the alloy system in view of their high melting point and hardness. However, inferior wetting characteristics of SiC with Al melt and differential thermal expansion coefficient of the two make the Al/SiC interface facilitate nucleation of microcracks and their subsequent propagation in the material system. This imparts cracking tendency in the composite. The composite in this case does not allow load transfer from the matrix to the SiC particles leading to premature pull out/removal of the particles during testing causing inferior performance of the composite material. This behaviour becomes predominant at lower temperatures. The overall influence of the SiC dispersoid thus is controlled by the nature predominance of one set of characteristics of composite leading to improved performance/characteristics over the other producing a reverse influence. At lower temperatures, cracking tendency imparted by the SiC particles predominates while lower strain rates also produce an identical influence in view of the availability of sufficient time to allow these processes to occur during loading. On the contrary, the cracking tendency gets suppressed with increasing temperature in view of improved compatibility of the dispersoid with that of the matrix alloy emanating from increased viscoplasticity of the latter. Under the circumstances, the SiC particles become more effective in realizing load transfer by way of their better retention by the matrix ultimately leading to improved performance. Higher strain rates help reduce the time available for the occurrence of the negative effect of the SiC particles causing improved response. Accordingly, the overall response of the composite is controlled by the operating conditions and is reflected depending on the nature of predominance of one set of factors leading to deterioration in performance over the other producing a reverse influence. Accordingly, the lower flow stress of the composite compared to that of the matrix alloy

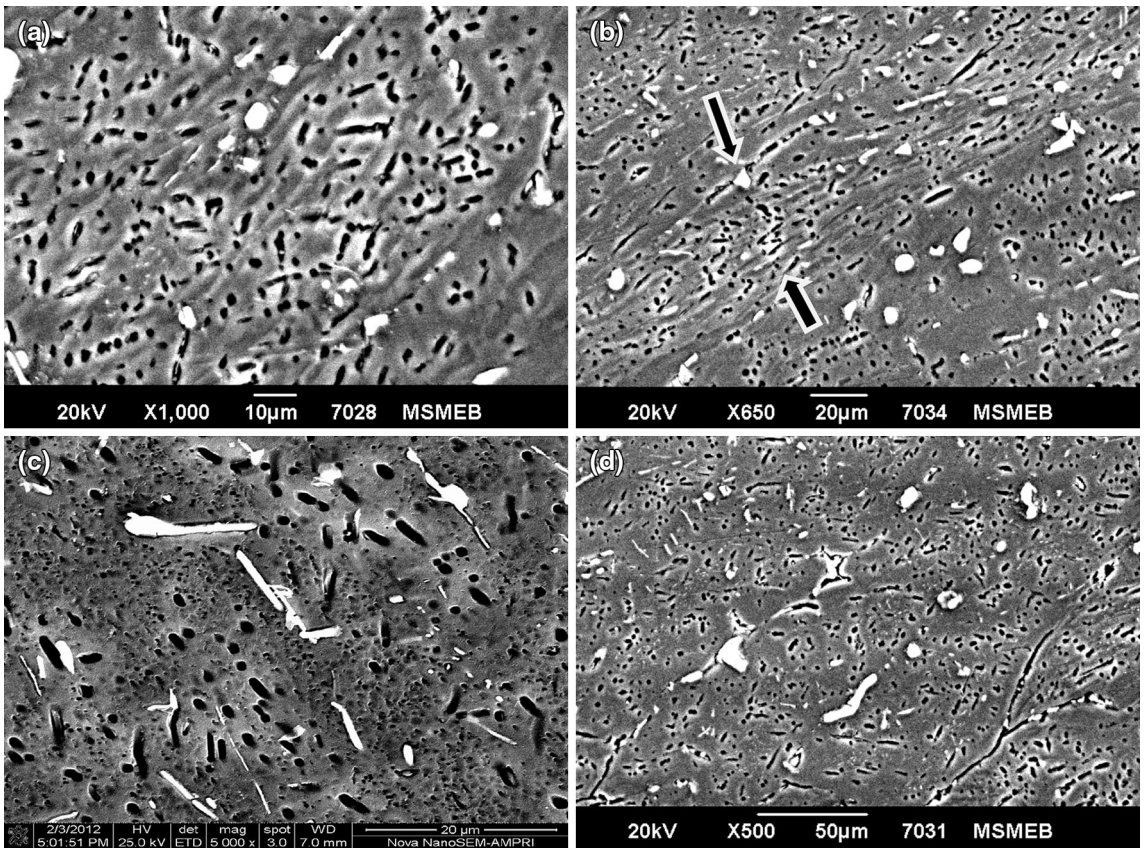

Fig. 4 **a** Typical optical micrograph of AA2014 alloy deformed at temperature of 30 °C and 0.01/s strain rate. **b** Typical optical micrograph of AA2014 alloy deformed at temperature of 30 °C and 10/s strain rate. **c** Typical micrograph of AA2014 alloy deformed at temperature of 400 °C and 0.01/s strain rate. **d** Typical micrograph of AA2014 alloy deformed at temperature of 400 °C and 10/s strain rate

could be attributed to the predominant negative effect of segregation of the dispersoid (SiC) particles and SiC/matrix interfacial cracking tendency in the case of the former as is also obvious from the microstructure of the deformed samples (Fig. 5e, f).

Initially high rate of increase in stress with increasing strain (Figs. 1, 2) could be attributed to the substantial extent of work hardening effect of the deforming matrix (alloy) while a reversal in the trend is due to (the predominant effect of) work softening; a balance between the counteracting influences of work hardening and softening makes the samples display steady state flow behaviour beyond the peak stress. The face centered structure of Al makes it prone to work hardening in view of a substantial number of slip systems and high stacking fault energy associated with the element thus facilitating cross slip to occur. Increase in the flow stress with strain rate could be attributed to the non-availability of time for the defects to show their negative influence in view of shorter test durations. On the contrary, a reduction in the flow stress with rising temperature emanates from the increasing mobility and subsequent annihilation of dislocations and material softening. Comparable strength of the composite with that of the matrix alloy suggests a counterbalancing effect of the cracking tendency and load bearing capability of the dispersoid SiC phase in the alloy matrix. That compression test could be conducted up to low strains only in the case of the composite at lower temperatures. This could be attributed to its substantial cracking tendency as discussed earlier. The cracking tendency got suppressed gradually with increasing temperature thus enabling the samples to be tested for larger strains. The softening behaviour of the samples at higher temperatures is also evident from the formation of fine equiaxed DRX grains in the (matrix) alloy (Fig. 5h) and a corresponding reduction in the activation energy (Fig. 6).

Better deformability characteristics of the matrix alloy compared to that of the composite (Figs. 1, 2) could be attributed to increased efficiency of power dissipation (Fig. 3a vs b), lower activation energy (Fig. 6a vs b) and more tendency towards the formation of DRX grains (Fig. 4f vs 5h). It may be mentioned that the presence of hard SiC particles restricts the flow of the matrix part of the material in case of the composite by impeding the movement of dislocations which when exceeds a limit gives rise to material cracking preferably appearing as dispersoid/matrix interfacial cracking (Fig. 5d, e), thus adversely

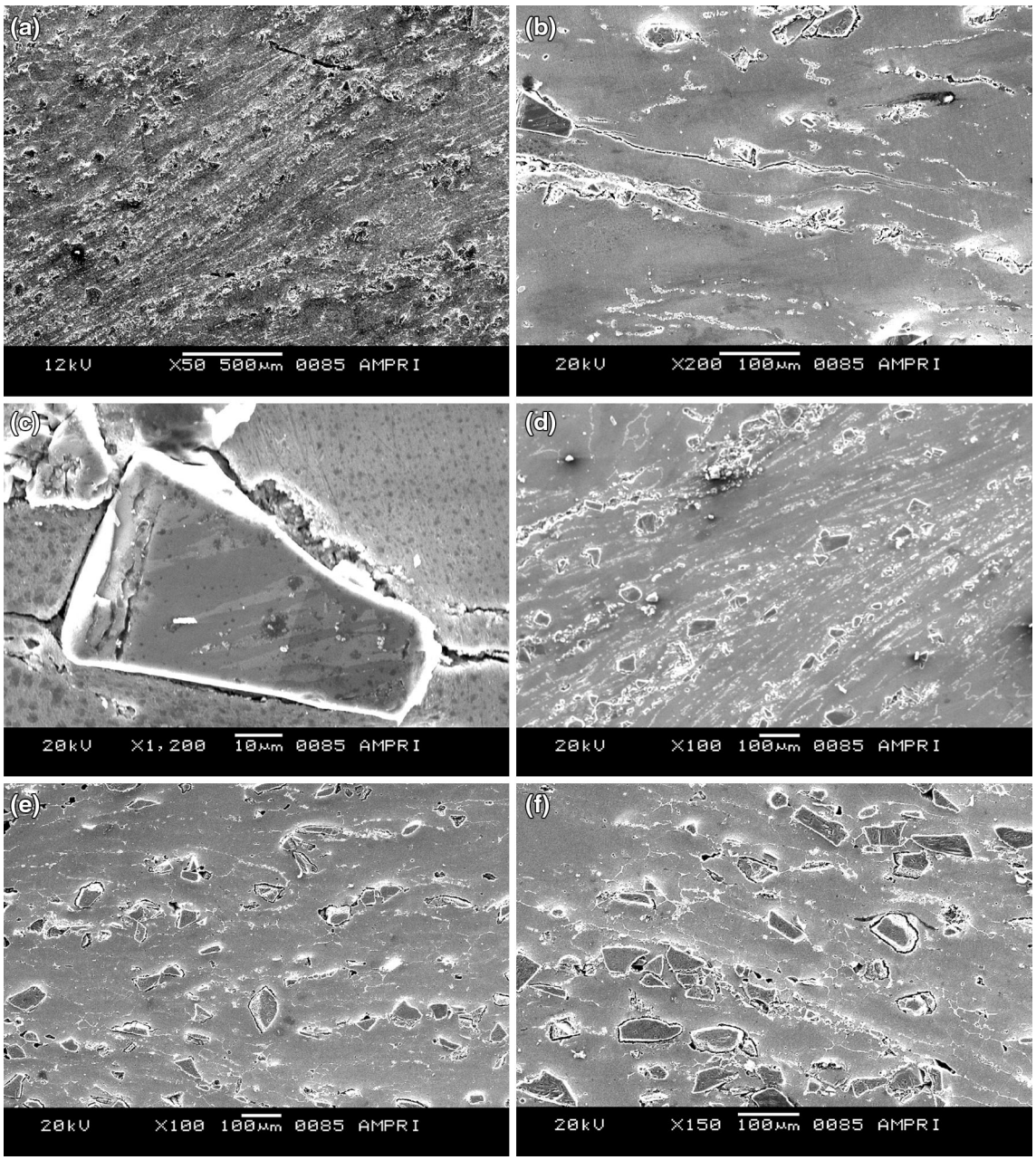

Fig. 5 **a** Typical scanning electron micrograph of AA2014–10 % SiC composite deformed at temperature of 30 °C and 0.01/s strain rate. **b** Typical scanning electron micrograph of AA2014–10 % SiC composite deformed at temperature of 30 °C and 0.01/s strain rate. **c** Typical scanning electron micrograph of AA2014–10 % SiC composite deformed at temperature of 30 °C and 0.01/s strain rate. **d** Typical scanning electron micrograph of AA2014–10 % SiC composite deformed at temperature of 30 °C and 10/s strain rate. **e** Typical scanning electron micrograph of AA2014–10 % SiC deformed at temperature of 400 °C and 10/s strain rate. **f** Typical scanning electron micrograph of AA2014–10 % SiC composite deformed at temperature of 400 °C and 0.01/s strain rate

affecting the deformability property. The instability was mainly due to flow localization of Al grains along with wedge cracking at grain boundaries (Fig. 4d, e). In the case of the composite, flow localization (Fig. 5c, f) was associated with the cracking tendency imparted by the dispersed SiC particles (Fig. 5d, e). It may be mentioned that load accumulation takes place at the interface of SiC and ductile matrix and leads to interfacial decohesion during the process of deformation. In some instances, particle fracture due to load accumulation was also discernible. However, at high temperatures, grain flow occurred due to softening of the matrix in view of DRX grain formation.

The Zener–Hollomon parameter Z was calculated using the following relation [33]:

$$Z = \dot{\epsilon}^{(Q/RT)} \tag{3}$$

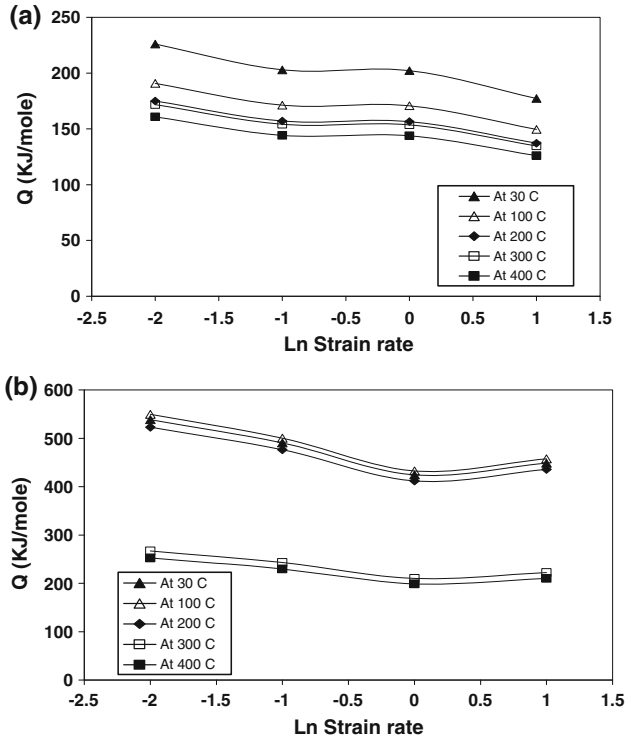

Fig. 6 **a** Activation energy of Al alloy, **b** Activation energy of Al composite

where $\dot{\varepsilon}$, Q, R and T represent strain rate, activation energy for deformation, ideal gas constant (R = 8.314 J/mol K) and the deformation temperature. The physical meaning of Z is temperature compensated/modified strain rate parameter. The Ln Z parameter for the alloy and composite at different temperatures and strain rates are shown in Tables 1 and 2, respectively. It is observed from the table that Ln Z values decreases with increasing temperature. Comparing the Ln Z values, it is found that composite has higher Ln Z values than that of the alloy at all temperatures and strain rates.

Reduction in the activation energy with temperature (Fig. 6) could be attributed to increased viscoplasticity of the matrix thus facilitating better flow. In the case of the alloy, softening behaviour of the matrix due to DRV and recrystallization as well as stress relaxation at the precipitate/matrix interface leads to a decrease in the activation energy [34, 35]. At lower temperatures, low ductility of the matrix gives rise to cracking tendency at the precipitate/matrix interface which becomes the dominant material failure mechanism. In the case of the composite, dispersoid/matrix interfacial decohesion/ cracking further aggravates the situation. Cracking tendency in the material system becomes prominent at lower strain rates of deformation wherein enough time becomes available for the cracks/voids to nucleate and propagate. An increase in the strain rate within limits causes the activation energy to be more or less constant (Fig. 6). This clearly indicates that the defects do not get enough time to nucleate and propagate effectively as at lower strain rates. Increasing strain rate beyond a limit facilitates crack to propagate to failure of material. The observed variation in the activation energy (126–538 kJ/mol) over the entire range of test conditions for the matrix alloy and composite falls close to the one reported earlier [36, 37]. In the case of AA2014, the activation energy at 400 °C is found to be in the range of 126–160 kJ/mol while the microstructural features revealed initiation of

Table 1 LnZ values under different deformation condition for AA2014 alloy

Temperatures (°C)	Strain rates/s			
	0.01	0.1	1	10
30	41.66566	42.66566	43.66566	44.66566
100	33.47103	34.47103	35.47103	36.47103
200	25.97187	26.97187	27.97187	28.97187
300	21.09022	22.09022	23.09022	24.09022
400	17.65928	18.65928	19.65928	20.65928

Table 2 LnZ Values under different deformation condition for AA2014–10 % SiC composite

Temperatures (°C)	Strain rates/s			
	0.01	0.1	1	10
30	62.40869	64.71169	67.01369	69.31569
100	49.83239	52.13539	54.43739	56.73939
200	38.32343	40.62643	42.92843	45.23043
300	30.83156	33.13456	35.43656	37.73856
400	25.5661	27.8691	30.1711	32.4731

wedge cracking near the grain boundary triple points and recrystallized grains. Grain boundary diffusion is also expected to be active in this case [38]. At higher temperatures and strain rates, the mechanism of deformation is adiabatic heating, cracking and flow localization. Higher activation energy for the composite than that of matrix alloy (Fig. 6b vs a) could be attributed to the presence of precipitates and SiC particles that give rise to stress accumulation around them and subsequently to cracking on exceeding a critical stress value. The precipitates and SiC particles make dislocation climb as the rate controlling step during the deformation of Al MMCs [34].

5 Conclusions

(1) The flow stress increased with strain initially at a higher rate and attained a peak value. This was followed by the attainment of a steady state condition at still higher strain levels. In some cases, the flow stress underwent a subsequent reduction beyond the peak while a slower rate of further increase in the flow stress was noted in other test conditions as the strain was increased after attaining the peak stress. The nature of the plot beyond the peak was controlled by the nature of predominance of work hardening over work softening; the test conditions like strain rate and temperature playing an important role in this context.

(2) Broadly speaking, the flow stress of the composite was comparable to that of the matrix alloy. However, the strain to which the composite could be deformed, especially at low temperatures, was much less than that of the matrix alloy.

(3) The safe domains for the hot working of alloy were comparable to that of composite. For example, the efficiency of power dissipation leading to microstructural evolution was much higher for the alloy than that of the composite. The superplastic deformation and DRX zones corresponding to optimum working region are identified. For example, the optimum processing regions in case of the alloy was found to lie in the temperature range of 350–400 °C and strain rate 0.01–0.1/s with an efficiency of 55 % while it became 250–400 °C and 0.01–0.1/s with the efficiency of 10–26 % for the composite.

(4) Microstructural investigation of the deformed alloys exhibited elongated grains of ductile Al with $CuAl_2$ phase along the grain boundaries in a direction perpendicular to that of compression axis. The dispersed SiC particles got surrounded with Al grains and flowed along with the latter. During the process of deformation, SiC particles participated in load transfer from the matrix as evident from the retention and fracture of the particles therein.

(5) Softening of the matrix through DRV/recrystallization is the main reason for the flow softening during deformation at high temperatures. On the contrary, decohesion of particles with the matrix was responsible for strain localization at high strain rates. High strain rates and low temperatures led to the generation of heat due to the local temperature rise that could not be dissipated away because of high speed of deformation. This resulted into the formation of adiabatic shear bands that ended up with cracking of material.

(6) The important material failure mechanism is the dispersoid/matrix and precipitate/matrix interfacial cracking at low temperatures. With the increase of temperature, the cracking tendency reduced and dispersoid and the precipitate tended to take part in the process of deformation in view of increase viscoplasticity of the matrix.

(7) The activation energy for the deformation of the matrix alloy was found to be in the range of 126–226 kJ/mol. This is significantly less than that of the composite (210–538 kJ/mol). This indicates that SiC particles restrict the flow of the matrix. The activation energy reduced with increasing temperature while strain rate produced a mixed influence.

Acknowledgments This work has been carried out under the Network Project NWP-0028 of Council of Scientific and Industrial Research, New Delhi India. Authors thank Mr. Sasi Bhusan and Mr. Prasanth N for extending the facilities for compression tests.

References

1. Lloyd D J, *Int Mater Rev* **39** (1994) 1.
2. Hunt W H, *J Met* **45** (1993) 18.
3. Miracle D B, and Donaldson S L, *Composites Handbook. ASM Handbook*, Vol 21, The Material Information Society, Materials Park (2001).
4. Rohatgi P K, *JOM* **43** (1991) 10.
5. Nussbaun A J, *Light Metal Age* **53** (1997) 54.
6. Rawal S, *JOM* **14** (2001) 14.
7. Karamis M B, Tasdemirci A, and Nair F, *Compos Part A* **34** (2003) 217.
8. Su H, Gao W, Feng Z, and Lu Z, *Mater Des* **36** (2012) 590.
9. Sajjadi S A, Parizi M T, Ezatpour H R, and Sedghi A, *J Alloy Compd* **511** (2012) 226.
10. Geiger A L, and Walker J A, *JOM* **43** (1991) 8.
11. Marsden K, *JOM* **37** (1985) 59.
12. Li Y, and Langdon T G, *J Mater Sci* **35** (2000) 1201.
13. Valiev R Z, Islamgaliev R K, Kuzmina N F, Li Y, and Langdon T G, *Scripta Mater* **40** (1999) 117.
14. Mitra R, Rao V S C,Maiti R, and Chakraborty M, *Mater Sci Eng A* **379** (2004) 391.
15. Sharma M M, Amateau M F, and Eden T J, *Mater Sci Eng A*, **425** (2006) 87.
16. Hong S H, Chung K H, and Lee C H, *Mater Sci Eng A* **206** (1996) 225.
17. Prasad Y V R K, and Sasidhara S, *Hot Working Guide—A Compendium of Processing Maps*, ASM International Publisher, Materials Park (1997).

18. Raj R, *Metal Trans A* **12** (1981) 1089.
19. Gandhi C, *Metall Trans* A **13** (1982) 1233.
20. Gandhi C, and Raj R, *Metall Trans A* **12** (1981) 515.
21. Bhat B V R, Mahajan Y R, Roshan H, and Prasad Y V R K, *Mater Sci Technol* **11** (1995) 167.
22. Bhat B V R, Mahajan Y R, and Prasad Y V R K, *Metal Mater Trans A* **31** (2000) 629.
23. Xia X, Sakaris P, and McQueen H J, *Mater Sci Technol* **10** (1994) 487.
24. Vedani M, Errico F D, and Gariboldi E, *Compos Sci Technol* **66** (2006) 343.
25. Cerri E, Spigarelli S, Evangelista E, and Cavaliere P, *Mater Sci Eng A* **324** (2002) 157.
26. Bhat B V R, Mahajan Y R, Roshan H, and Prasad Y V R K, *Mater Sci Eng A* **189** (1994) 137.
27. Murty N S V S, Nageswara Rao B, and Kashyap B P, *J Mater Process Technol* **166** (2005) 279.
28. Shao J C, Xiao B L, Wang Q Z, Ma Z Y, Liu Y, and Yang K, *Mater Sci Eng A* **527** (2010) 7865.
29. Ganesan G, Raghukandan K, Kartheikeyan R, and Pai B C, *Mater Sci Eng* A **369** (2004) 230.
30. Bhat B V R, Mahajan Y R, and Prasad Y V R K, *Metall Mater Trans A* **31** (2000) 629.
31. Ramanathan S, Karthikeyan R, and Ganesan G, *Mater Sci Eng A* **441** (2006) 321.
32. Xiao B L, Fan J Z, Tian X F, Zhang W Y, and Shi L K, *J Mater Sci* **40** (2005) 5757.
33. Patel A, Das S, and Prasad B K, *Mater Sci Eng A* **530** (2011) 225.
34. Malas J C, Venugopal S, and Seshacharyullu T, *Mater Sci Eng* A **368** (2004) 41.
35. Koike J, Mabuchi M, and Higashi K, *Acta Metall* **43** (1995) 199.
36. Csetenyi E K, Chinh N Q, and Kovacs I, *Phys Stat Solidi* **148** (1995) 135.
37. Iwasaki H, Mori T M, Mabuchi, and Higashi K, *Mater Trans* **41** (2000) 367.
38. Frost H J, and Ashby M F, *Deformation Mechanism Maps*, Pergamon, Oxford (1982), p 21.